Hindawi
International Journal of Energy Research
Volume 2024, Article ID 6662859, 17 pages
https://doi.org/10.1155/2024/6662859

Research Article

Preparation and Performance of Inorganic Hydrated Salt-Based Composite Materials for Temperature and Humidity Regulation

Rongda Ye,[1] **Jun Wang**,[1] **Yanna Li**,[1] **Wanchun Sun**,[2] **Xuelin Zou**,[3] **Fangxian Wang**,[4] **and Xugang Shu**[1]

[1]*School of Chemistry and Chemical Engineering, Zhongkai University of Agriculture and Engineering, Guangzhou 510225, China*
[2]*School of Energy and Automotive Engineering, Shunde Polytechnic, Foshan 528300, China*
[3]*Guangdong Provincial Key Laboratory of Distributed Energy Systems, School of Chemical Engineering and Energy Technology, Dongguan University of Technology, Dongguan 523808, China*
[4]*Research Center for Eco-Environmental Engineering, Dongguan University of Technology, Dongguan 523808, China*

Correspondence should be addressed to Rongda Ye; ye-rongda@outlook.com

Received 25 July 2023; Revised 30 November 2023; Accepted 15 March 2024; Published 16 April 2024

Academic Editor: Saleh N. Al-Saadi

In this work, it was first proposed to combine hydrated salt phase change materials (PCMs) with humidity control materials to prepare the temperature and humidity control material. The composite PCM was prepared by absorbing $Na_2HPO_4{\cdot}12H_2O$ with colloidal silicon dioxide, and diatomite was selected as the humidity control material. The humidity performance tests found that diatomite had good moisture absorption/desorption capacity and excellent moisture buffering capacity. The supercooling degree tests showed that $Na_2SiO_3{\cdot}9H_2O$ as nucleating agent effectively reduced the supercooling degree, and the addition of deionized water improved the water loss problem of composite PCMs. The DSC tests showed that the enthalpy and melting temperature of composite PCMs were 153.1 J/g and 28.9°C, respectively. By placing the temperature and humidity control material in different humidity, it was found that the moisture content of diatomite affected the thermal properties of composite PCMs. Diatomite could not only transfer moisture to hydrated salts but also absorb moisture from hydrated salt. The application performance tests of the temperature and humidity control material in the room model showed that it could simultaneously regulate indoor temperature and humidity. Overall, this temperature and humidity control material was more suitable for environments with high relative humidity such as greenhouses.

1. Introduction

Temperature and humidity are two important environmental parameters, which will not only affect the comfort and health of residents and animals but also affect the growth of crops [1–3]. At present, mechanical equipment such as HVAC and dehumidifiers is mainly used to control temperature and humidity to achieve a stable and comfortable environment, which leads to a large amount of energy consumption and carbon dioxide emissions [4, 5]. For buildings such as houses or greenhouses, temperature and humidity are mainly transmitted and diffused through the building envelope. Therefore, it is necessary to give full play to the characteristics of different materials and endow building structures with functions such as temperature and humidity regulation.

The thermal environment mainly depends on the thermal insulation capacity of the building envelope. Lightweight building materials generally have the disadvantage of small heat capacity, which is easy to cause large fluctuations in indoor temperature [6, 7]. Phase change materials (PCMs) have a large heat storage capacity. The thermal energy can be effectively stored and released using its phase change characteristics, which is expected to achieve the regulation of the thermal environment [8–10]. A large number of literatures have reported that PCMs can be integrated into building envelopes [11–13]. The reasonable structure design reduced the temperature fluctuation and improved thermal

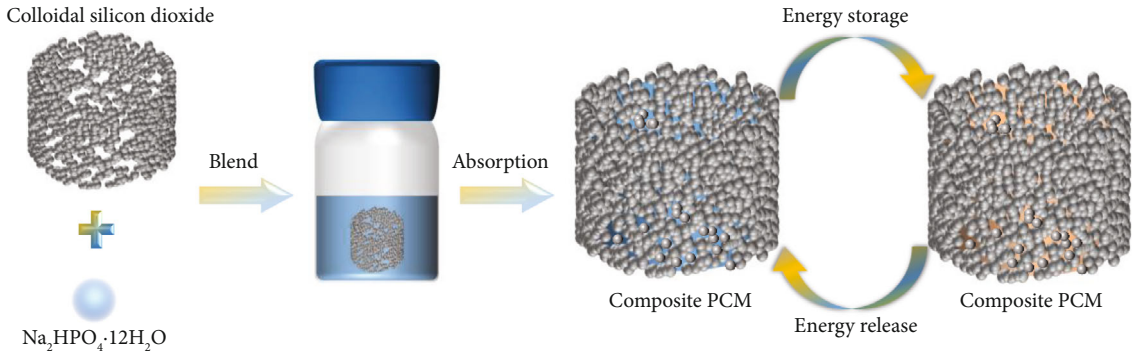

Figure 1: Schematic diagram of the preparation process of composite PCMs.

comfort, which was conducive to reducing energy consumption and rationalizing energy use. In terms of humidity environment regulation, the commonly used active regulation methods (such as dehumidifiers) do not meet the requirements of energy conservation and emission reduction. For the passive humidity control method, the indoor humidity is adjusted by virtue of the moisture absorption and desorption characteristics of the humidity control materials [14, 15]. Inorganic porous materials have become one of the best humidity control materials due to their large specific surface area and pore volume [16–18]. Without any artificial energy or mechanical equipment, it can automatically sense the changes of ambient air humidity, thereby improving the humidity environment. It was well known that PCMs and humidity control materials could improve the thermal environment and humidity environment, respectively, but they need to be effectively combined to achieve the purpose of regulating temperature and humidity simultaneously.

In recent years, composite materials with temperature and humidity regulating functions have been reported in the literature [19–21]. It was found that PCMs and humidity control materials could be combined in proper forms to improve the temperature and humidity environment simultaneously, which was an effective way to achieve efficient energy utilization. Wang et al. [22] used sepiolite-zeolite as humidity control materials and capric acid microcapsules as PCMs to prepare the composite material with temperature and humidity regulating functions. The results showed that the composite material reduced the temperature fluctuation by 2~3°C and maintained the relative humidity (RH) between 51.75 and 58.84%. Chen et al. [23] prepared hygroscopic PCMs by mixing microencapsulated PCMs with diatomite. The enthalpy and moisture buffer values (MBV) of the composite material obtained were 19 J/g and 1.57 g/(m^2·%RH), respectively, which had the ability to adjust the indoor temperature and humidity. Park et al. [24] improved the hygrothermal performance of gypsum by adding porous materials (expanded vermiculite, expanded perlite, and carbon nanomaterials) and PCMs. In addition, the functional gypsum board had high thermal insulation and heat storage capacity, and there was no moisture problem. Zong et al. [25] employed Ce-Eu/TiO_2 hollow microspheres as carriers to adsorb organic eutectic PCMs, and the resulting composite materials had the thermal-humidity-photocatalysis synergistic performance. Specifically, its enthalpy was 64.6 J/g. The moisture capacity under 43.16~75.29%RH was 0.0575 g/g. The degradation rate of gaseous formaldehyde reached 54.98% after 5 h. Hou et al. [26] prepared a hygrothermal control material with dual functions, which used microencapsulated PCMs and metal-organic frameworks as temperature and humidity control materials, respectively. The numerical results showed that the composite material significantly reduced indoor temperature and humidity fluctuations compared with the gypsum board. Gonçalves et al. [27] reported the preparation of highly porous bilayered alkali-activated composite materials containing microencapsulated PCMs. The results showed that it delayed the minimum temperature of the room for 1 h and reduced the temperature fluctuation by 1.5°C. It also had the function of buffering humidity, and the MBV was 2.71 g/(m^2·%RH). The existing researches have confirmed that the temperature and humidity control material could not only use renewable energy such as solar energy or cold air at night for heat or cold storage but also absorb or release moisture timely according to the change of environmental relative humidity. However, the research on temperature and humidity control materials was still in its infancy. In addition, due to the good stability of organic PCMs, the existing research was based on the combination of organic PCMs and humidity control materials, which played their own role without interaction.

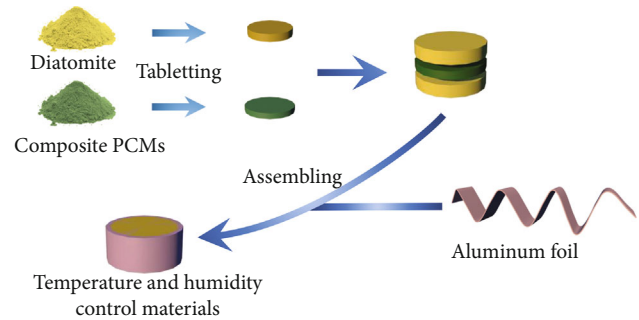

Figure 2: Schematic diagram of the preparation process of temperature and humidity control materials.

PCMs are generally divided into organic PCMs and inorganic PCMs [28]. Compared with organic PCMs (paraffin,

Table 1: The RH of air above saturated solution under equilibrium conditions.

Temperature (°C)	RH (%)			
	$MgCl_2$	$Mg(NO_3)_2$	NaCl	K_2SO_4
25	32.78 ± 0.16	52.89 ± 0.22	75.29 ± 0.12	97.30 ± 0.45
30	32.44 ± 0.14	51.40 ± 0.24	75.09 ± 0.11	97.00 ± 0.40

fatty acid, etc.), inorganic PCMs, such as inorganic hydrated salts, are cheaper and nonflammable, so they will have a wider application prospect. However, inorganic hydrated salts suffer from phase instability, supercooling, issue of corrosion and vaporization, and low optical absorbance [29–31]. Especially the problems of phase instability and supercooling can affect the thermal properties of PCMs, but these issues can be resolved through appropriate methods [32–35]. The inorganic hydrated salt PCM is composed of inorganic salts and water molecules. Although preparing composite PCMs can solve the problem of liquid leakage during the phase change process, its thermal characteristics will still be affected by air humidity [36, 37]. For example, when $CaCl_2{\cdot}6H_2O$ is directly exposed to the air, it will deliquesce due to absorption of air moisture. On the contrary, $Na_2HPO_4{\cdot}12H_2O$ easily loses its water molecules. Both inorganic hydrated salt composite PCMs and humidity control materials can absorb or release moisture, so it can be inferred that there will be a coupling effect between them. However, up to now, the investigation on the combination of inorganic hydrated salt composite PCMs and humidity control materials has not been reported, and the interaction between them is still unclear.

In this work, a composite PCM was prepared by using colloidal silicon dioxide as the support carrier and $Na_2HPO_4{\cdot}12H_2O$ as inorganic hydrated salts. Then, it was combined with diatomite, which was employed as the humidity control material to prepare a temperature and humidity control material with the sandwich structure. The equilibrium moisture absorption/desorption content and moisture buffer value of the humidity control material were measured using desiccators, and the dynamic curve of moisture absorption/desorption was obtained. The pore structure, particle size distribution, micromorphology and structure, supercooling degree, and thermal stability of the material were tested and characterized. The phase change temperature and enthalpy of composite PCMs in the sandwich structure after being placed in different RH for different days were measured and compared. The results confirmed an interaction between inorganic hydrated salt composite PCMs and humidity control materials. In addition, the potential application of this temperature and humidity control material in the room model had been studied. The results indicated that it helped improve the indoor temperature and humidity environment. The obtained temperature and humidity control materials have potential applications in high humidity environments such as greenhouses.

2. Experimental Section

2.1. Materials. Disodium hydrogen phosphate dodecahydrate ($Na_2HPO_4{\cdot}12H_2O$, AR) was obtained from Shanghai Aladdin Biochemical Technology Co., Ltd. Sodium metasilicate nonahydrate ($Na_2SiO_3{\cdot}9H_2O$, AR) was obtained from Sinopharm Chemical Reagent Co., Ltd. Colloidal silicon dioxide ($mSiO_2{\cdot}nH_2O$) was purchased from Shandong Yousuo Chemical Technology Co., Ltd. Diatomite was purchased from Hebei Huakai Environmental Protection Materials Co., Ltd.

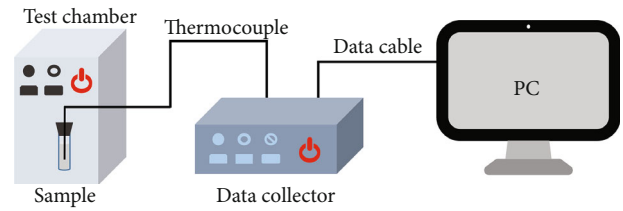

Figure 3: Schematic diagram of the supercooling degree test system.

2.2. Preparation of Composite PCMs. Firstly, deionized water and $Na_2HPO_4{\cdot}12H_2O$ were added into a sealable bottle. After $Na_2HPO_4{\cdot}12H_2O$ was completely dissolved at 50°C, $Na_2SiO_3{\cdot}9H_2O$ as the nucleating agent was added. After the above mixture was stirred evenly, colloidal silicon dioxide with a mass fraction of 30% was poured into the bottle, and then, they were stirred with a glass rod. In the process of stirring, intermittent heating was required to keep $Na_2HPO_4{\cdot}12H_2O$ in the melting state, which was conducive to the full adsorption of $Na_2HPO_4{\cdot}12H_2O$. When the mixture was fully stirred, it was cooled to room temperature to obtain composite PCMs. The preparation process of composite PCMs is shown in Figure 1.

2.3. Preparation of Temperature and Humidity Control Materials. The preparation process of temperature and humidity control materials is shown in Figure 2. Firstly, diatomite and the composite PCM were pressed into the cylinder with a diameter of 18 mm. Then, the composite PCM was sandwiched between two pieces of diatomite to form a sandwich structure. The periphery and bottom of the sandwich structure were sealed with aluminum foil, leaving only one surface to contact with the external environment. To avoid the influence of gaps, a thin layer of the building structural adhesive was applied on the aluminum foil surface.

2.4. Characterization

2.4.1. Equilibrium Moisture Content Curves. The moisture absorption and desorption properties of diatomite were tested according to GB/T 20312-2006. First, diatomite was dried to constant weight in the oven. After it cooled down, it was placed in the weighing bottle. For the moisture

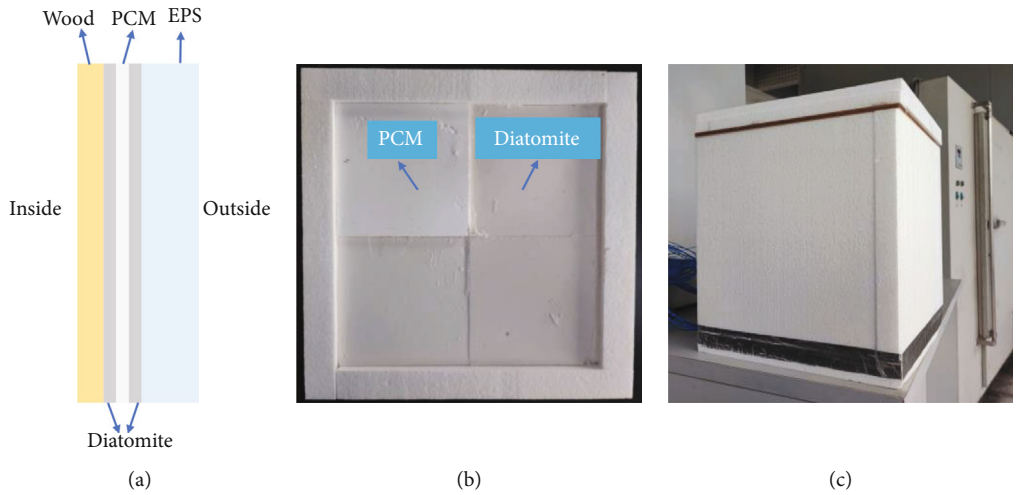

Figure 4: The structure of the roof (a); physical graphic of the PCM layer and diatomite layer (b); schematic diagram of the room mode (c).

absorption process, the weighing bottles were placed in desiccators with relative humidity (RH) of 33%, 52%, 75%, and 97%, respectively. For the moisture desorption process, diatomite was first saturated at 97%RH and then put into desiccators with RH of 33%, 52%, and 75%, respectively. The RH was determined by the type of saturated salt solution in the desiccator, as shown in Table 1. The equilibrium moisture absorption/desorption content and the dynamic curve of moisture absorption/desorption could be obtained by recording the change of sample mass with time. The moisture content of diatomite was calculated according to the following formula:

$$\mathrm{MC} = \frac{|m_t - m_0|}{m_0}, \tag{1}$$

where MC is the moisture content of diatomite (g/g), m_t is the mass of diatomite at a certain moment (g), and m_0 is the mass of diatomite after drying in the oven (g).

2.4.2. Moisture Buffer Value (MBV). The sides and bottom of the diatomite were first sealed with aluminum foil. Then, a thin layer of the building structural adhesive was applied on the aluminum foil surface. The sample was put into a desiccator at 52%RH to achieve the balance of moisture absorption and desorption. Then, the sample was subjected to the moisture absorption and desorption cycle at 75% and 33%RH: the sample was placed at 75%RH for 8 h, then transferred to 33%RH for 16 h, and repeated several times until the moisture absorption and desorption process became stable. The sample mass needed to be weighed during the cycle. The MBV was calculated according to the following formula:

$$\mathrm{MBV} = \frac{\Delta m}{(A \bullet \Delta \mathrm{RH})}, \tag{2}$$

where Δm is the mass change of the sample after the cycle process becomes stable (g), A is the surface area of the sample exposed to humidity (m^2), and ΔRH is the difference

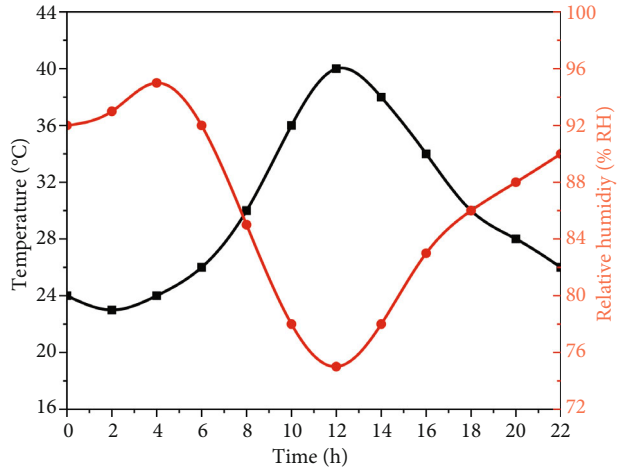

Figure 5: Temperature and humidity of the test chamber.

between high and low RH (%RH). The moisture buffer value, as an important indicator, is used to evaluate the moisture absorption and release performance of materials under periodic changes in relative humidity. The larger the moisture buffer value, the better the moisture absorption and release performance.

2.4.3. Pore Structure Analysis. The automatic specific surface area and porosity analyzer (Micromeritics ASAP 2460, USA) was selected to characterize the pore structure parameters of the sample. Based on nitrogen adsorption/desorption, the specific surface area was obtained by the Brunner–Emmet–Teller (BET) method. The pore distributions were obtained by the density functional theory (DFT) method. The specific surface area and pore volume of micropores were calculated by the t-plot method.

2.4.4. Supercooling Degree. The supercooling degree test system is shown in Figure 3. A sealed glass bottle was filled with compacted composite PCMs. It was placed in a high and low temperature alternating temperature humidity test chamber

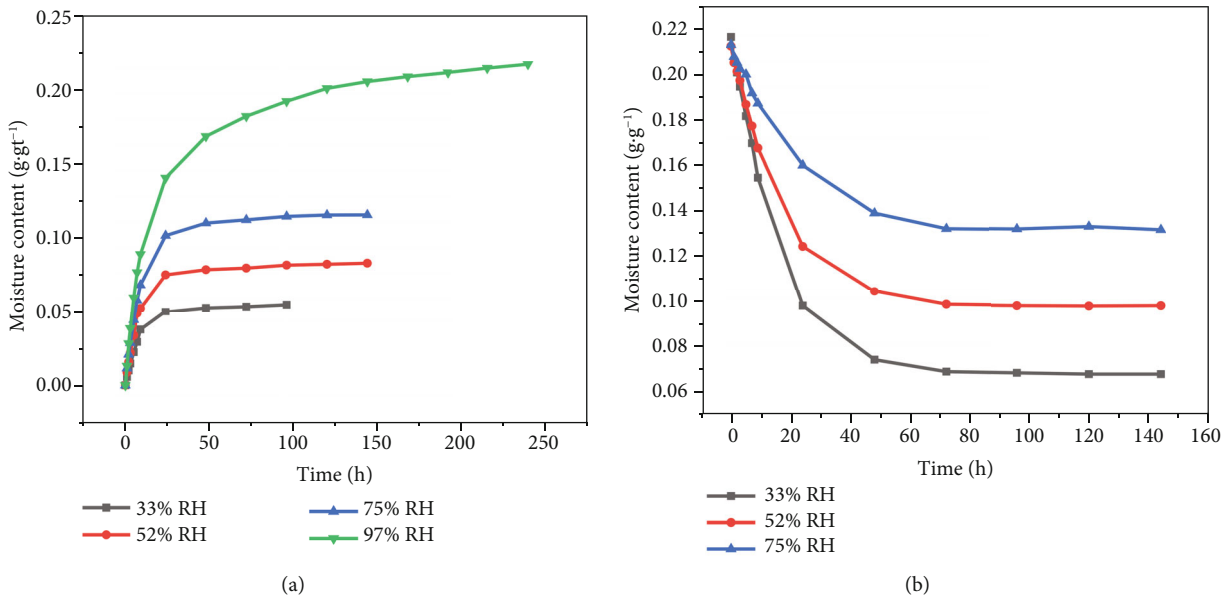

Figure 6: The dynamic curve of (a) moisture absorption and (b) moisture desorption.

(BPHJS-060B, Shanghai Yiheng Technology Instrument Co., Ltd., China) and connected to an Agilent 34970A data acquisition instrument through a thermocouple. The high temperature and low temperature of the test chamber were set at 50°C and 0°C, respectively. The temperature change of composite PCMs with time was recorded and saved by the computer.

2.4.5. Micromorphology and Structure. After the sample was sprayed with gold, the scanning electron microscope (SEM, Tescan MIRA LMS, Czech) was selected to observe its micromorphology. The chemical composition and structure of the samples were characterized by Fourier transform infrared spectroscopy (FT-IR, Nicolet iN10, USA). The crystal structure of the sample was tested and characterized by the X-ray diffractometer (XRD, Rigaku Ultima III, Japan) with a Cu target as the ray source at a scanning speed of 5°C/min.

2.4.6. TGA Test. The thermal stability and thermal decomposition of the sample could be characterized by the thermogravimetric analyzer (TGA, Mettler Toledo TGA2, Switzerland). The sample of about 10 mg was filled and sealed in a small aluminum crucible. The experiment was conducted under the nitrogen atmosphere at a heating rate of 10°C/min.

2.4.7. DSC Test. The thermal properties of composite PCMs, including phase change temperature, peak temperature, and latent heat, were measured by a differential scanning calorimeter (DSC, NETZSCH 214 Polyma, Germany). About 10 mg of the composite PCM was filled and sealed in a small aluminum crucible. The test process was protected by the nitrogen atmosphere, and the heating rate was 5°C/min.

All curves were plotted in Origin software. The schematic diagrams were drawn in Cinema 4D software.

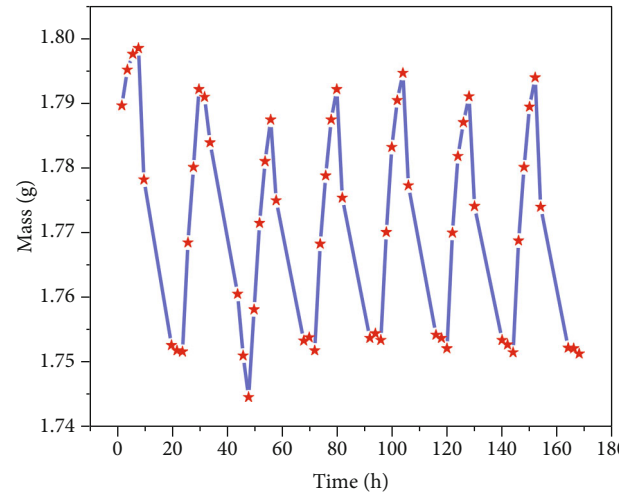

Figure 7: The change of diatomite mass with time in the process of moisture absorption and desorption cycle.

2.5. Construction of the Room Model. The size of the room model was 320 mm × 320 mm × 350 mm. The room without temperature and humidity control materials was named the reference room. It consisted of six EPS boards, two of which had a dimension of 320 mm × 320 mm × 30 mm for the floor and roof and the others had a dimension of 290 mm × 290 mm × 30 mm for the four walls. The room with temperature and humidity control materials was named the function room, which differed from the reference room in terms of roof structure. As shown in Figure 4(a), the roof was composed of wood, diatomite, PCM, diatomite, and EPS board from the inside out. The size of the internal wood was 320 mm × 320 mm × 5 mm. The diatomite layer and PCM layer were both composed of four small blocks with a size of 130 mm × 130 mm × 3 mm, as shown in Figure 4(b).

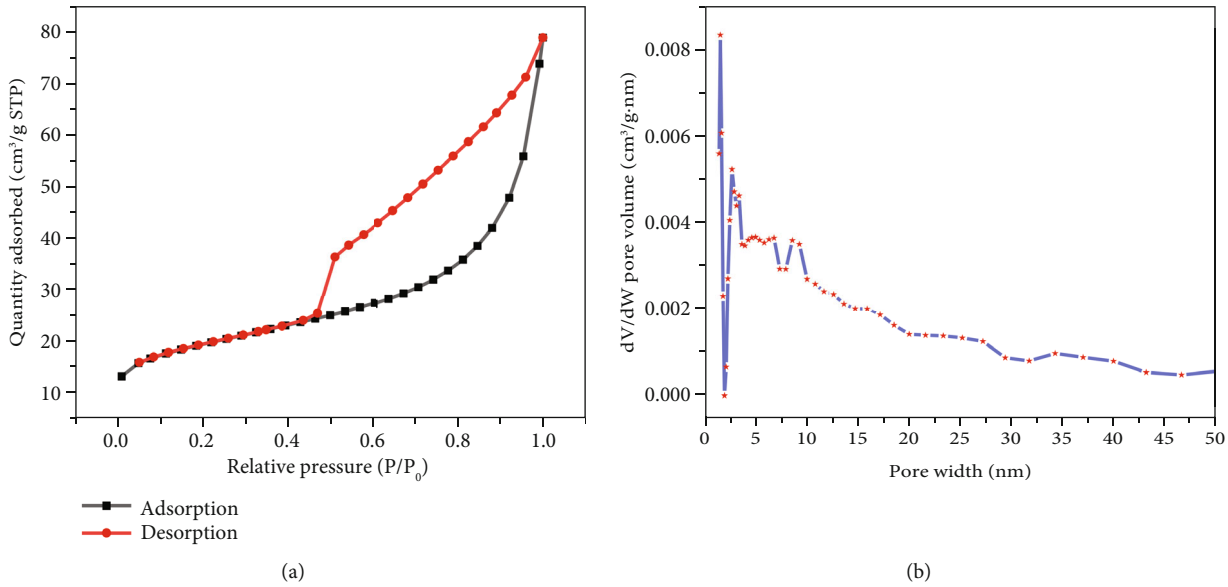

Figure 8: The (a) N_2 adsorption–desorption isotherms and (b) pore size distributions of diatomite.

Table 2: The pore structure parameters of diatomite.

Sample	S_{BET} (m^2/g)	S_{micro} (m^2/g)	V_t (cm^3/g)	V_{micro} (cm^3/g)	D (nm)
Diatomite	69.353	23.681	0.122	0.010	7.046

The size of the outer EPS board was 320 mm × 320 mm × 16 mm. The constructed room model is shown in Figure 4(c), and its hygrothermal performance was evaluated by placing it in a high and low temperature alternating temperature humidity test chamber. According to the summer climate in Guangzhou and the humidity characteristics of the greenhouse, the temperature and humidity settings in the test chamber are shown in Figure 5. The temperature and humidity recorder (RC-4HC) was employed to detect the temperature and humidity at the center of the inner surface of the roof, with a monitoring interval of 15 min.

3. Results and Discussion

3.1. Humidity Control Characteristics of Diatomite

3.1.1. Equilibrium Moisture Content Curves. The moisture content of diatomite at different times is shown in Figure 6. It can be seen from Figure 6(a) that diatomite had a fast moisture absorption rate. Its moisture content increased sharply within 24 h. After 48 h, the increase rate slowed down or remained unchanged. The equilibrium moisture content of diatomite at 33%RH, 52%RH, 75%RH, and 97%RH was 0.0546 g/g, 0.0828 g/g, 0.1155 g/g, and 0.2173 g/g, respectively. With the increase of RH, the equilibrium moisture content increased gradually. For the moisture release process, as shown in Figure 6(b), it can be seen that diatomite also had a fast moisture release rate. In the research work of Wang et al. [22], at 33%RH, the material only released about 30% of moisture within 24 h. In this work, the material could release about 30% of moisture in the first 9 h and about 60% of moisture within 24 h. When the moisture release process gradually reached equilibrium, the moisture content of diatomite at 33%RH, 52%RH, and 75%RH was 0.0686 g/g, 0.0989 g/g, and 0.1325 g/g, respectively. Compared with the equilibrium moisture content under the same RH during the moisture absorption process, it was only about 0.016 g/g higher, which indicated that diatomite could release most of the absorbed moisture. In general, the large moisture absorption/desorption rate was conducive to the rapid response of diatomite to the surrounding environment, while the large equilibrium moisture content endowed it with good moisture regulation capacity.

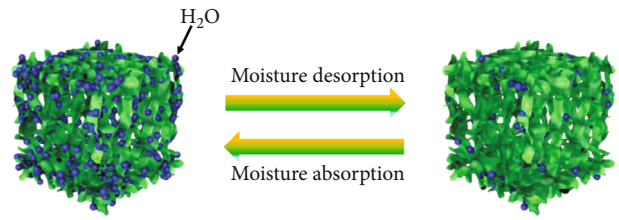

Figure 9: Schematic diagram of moisture absorption/desorption of diatomite.

3.1.2. Moisture Buffer Value (MBV). Figure 7 shows the moisture absorption and desorption performance of diatomite under the periodic change of relative humidity. It can be seen that the mass change of diatomite tended to be stable after the fourth cycle, which indicated that it could absorb and release moisture stably and repeatedly. When the

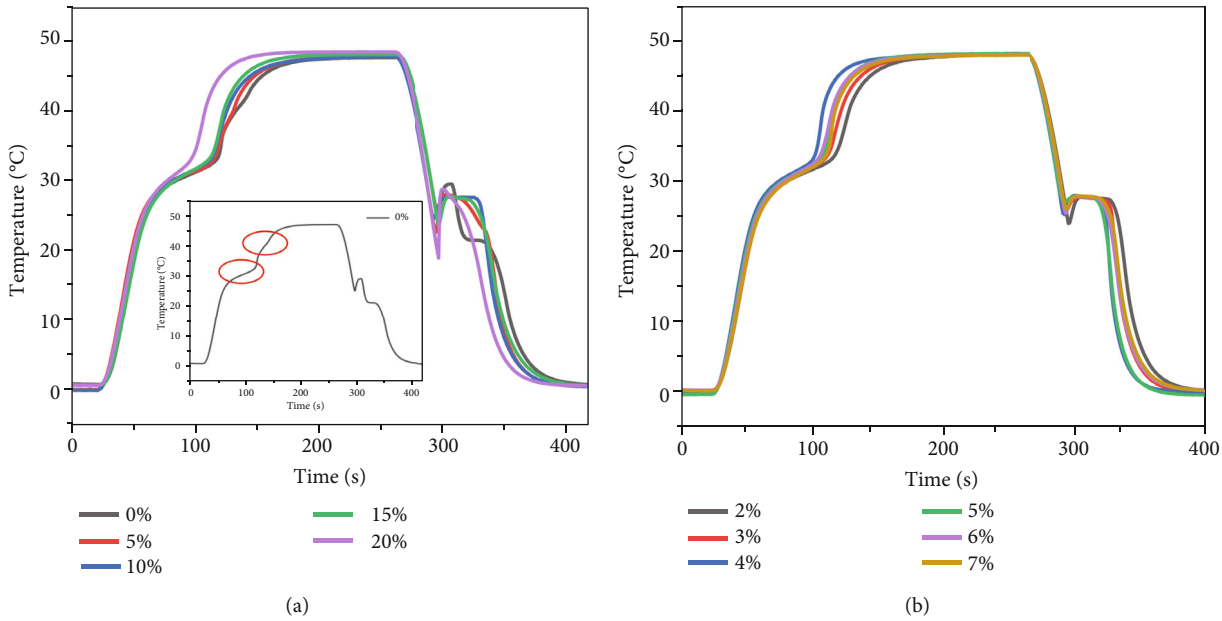

Figure 10: Cooling curves of composite PCMs: (a) without nucleating agent under different deionized water content; (b) with 10% deionized water under different nucleating agent content.

process was stable, MBV was calculated according to the mass change of diatomite, which was 3.81 g/(m^2·%RH). Based on the classification of MBV [27, 38, 39], when the MBV is greater than 2.00 g/(m^2·%RH), the humidity buffering performance of the material belongs to the excellent class. Therefore, the diatomite in this paper had excellent humidity regulation ability, which was helpful in controlling the humidity environment.

3.2. Pore Structure Analysis and Particle Size Distribution. The pore structure parameters and pore size distributions of diatomite were characterized by the N_2 adsorption-desorption isotherm. Based on the classification of IPUAC, as shown in Figure 8(a), it can be known that the adsorption-desorption isotherm of diatomite belonged to type IV isotherms. At low relative pressure ($P/P_0 < 0.1$), diatomite had a small nitrogen adsorption capacity, indicating that there were few micropores. When the relative pressure was between 0.47 and 1.00, an obvious H_3 hysteresis loop appeared, indicating that diatomite had a large number of mesopores. As shown in Table 2, the micropore volume of diatomite was only 0.010 cm^3/g, while the total pore volume was 0.122 cm^3/g. In addition, the specific surface area of micropores was 23.681 m^2/g. Based on BET analysis, the specific surface area was 69.353 m^2/g, which was much larger than that reported in other literatures [40–42]. The distribution of micropores and mesopores of diatomite is shown in Figure 8(b). It can be seen that the micropore size was mainly around 1.6 nm. The pore size distribution of mesopores was mainly distributed between 2 and 40 nm. The average pore diameter of diatomite was 7.046 nm. Abundant mesoporous structure and large specific surface area endowed diatomite with excellent humidity control ability. As shown in Figure 9, when the RH was high, a larger specific surface area improved the probability of moisture colliding with the diatomite particle surface and being adsorbed. In addition, capillary condensation mainly occurred in mesopores. The abundant mesoporous structure was conducive to absorbing and containing more moisture. When the RH was low, diatomite released most of the moisture it absorbed. Through the process of moisture adsorption and desorption, diatomite could adjust the ambient humidity.

Table 3: The supercooling degree of composite PCMs.

Material	Content (%)	Supercooling degree (°C)
Deionized water	5	5.4
	10	3.1
	15	4.2
	20	9.9
$Na_2SiO_3·9H_2O$	2	3.7
	3	2.0
	4	2.7
	5	0.8
	6	2.4
	7	1.8

3.3. Supercooling Degree. Without the nucleating agent, the cooling curves of composite PCMs with different deionized water content are shown in Figure 10(a), and the corresponding supercooling degree is shown in Table 3. It can be observed that when the deionized water content was 0%, there were two melting platforms for the composite PCM during the heating process, which was also found during the cooling process. When deionized water was added, the phenomenon was obviously improved. Therefore,

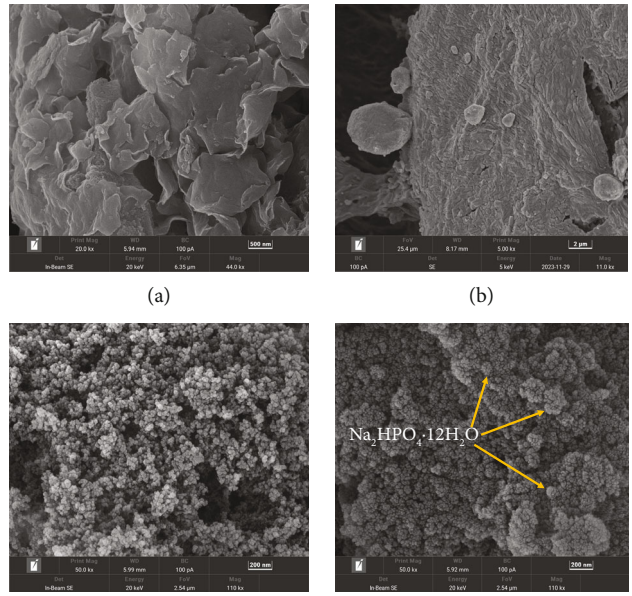

Figure 11: SEM images of samples: (a) diatomite; (b) $Na_2HPO_4{\cdot}12H_2O$; (c) colloidal silicon dioxide; (d) composite PCMs.

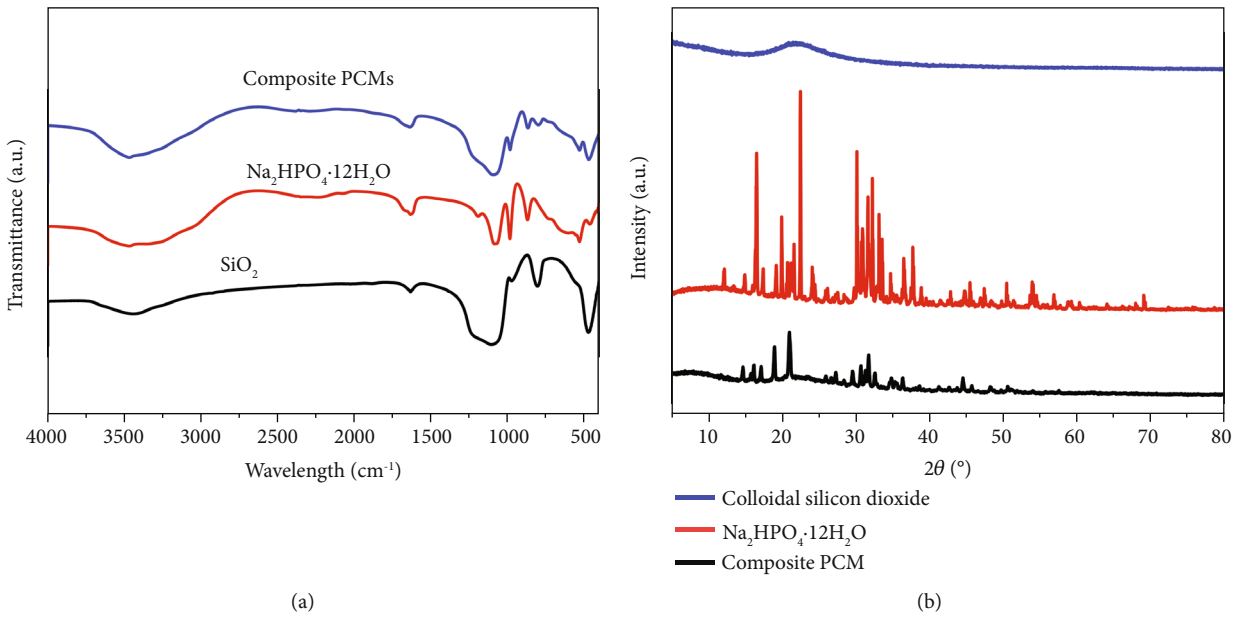

Figure 12: (a) FT-IR spectra and (b) XRD patterns of colloidal silicon dioxide, $Na_2HPO_4{\cdot}12H_2O$, and composite PCMs.

it was inferred that this phenomenon was caused by the water loss characteristics of $Na_2HPO_4{\cdot}12H_2O$. When the deionized water content was 5%, 10%, 15%, and 20%, the supercooling degree was 5.4°C, 3.1°C, 4.2°C, and 9.9°C, respectively. In the subsequent process, the content of deionized water was set at 10%, because the supercooling degree was minimum at this time.

The cooling curves of composite PCMs with different nucleating agent contents are shown in Figure 10(b). After adding $Na_2SiO_3{\cdot}9H_2O$ as the nucleating agent, the supercooling degree was further reduced. When the mass fraction of $Na_2SiO_3{\cdot}9H_2O$ was 2%, 3%, 4%, 5%, 6%, and 7%, the supercooling degree was 3.7°C, 2.0°C, 2.7°C, 0.8°C, 2.4°C, and 1.8°C, respectively. During the phase change process of PCMs, the nucleating agent remained in a solid state. These particles acted as crystal nucleus and provided nucleation sites, helping to promote the formation and growth of more crystal nucleus, thereby reducing the supercooling degree of PCMs [32, 43, 44]. When the content of nucleating agent was insufficient, it could not provide sufficient driving force and surface area to promote nucleation. When the content of nucleating agent was high, the viscosity of the system

increased, which led to particle aggregation and fewer nucleation sites. Therefore, to minimize the supercooling degree of the composite PCM, the appropriate amount of $Na_2SiO_3{\cdot}9H_2O$ was 5%.

3.4. Micromorphology and Structure. The micromorphology of the samples is shown in Figure 11. It can be seen from Figure 11(a) that diatomite had the rough surface and good porous structure, which could absorb moisture or other substances. For $Na_2HPO_4{\cdot}12H_2O$, it can be seen from Figure 11(b) that it exhibited lumped coarse crystals and the compact surface. For colloidal silicon dioxide, as shown in Figure 11(c), a large number of spherical particles were connected together to form a three-dimensional network structure. After colloidal silicon dioxide adsorbed $Na_2HPO_4{\cdot}12H_2O$, it can be seen from Figure 11(d) that the particles became larger and agglomerated together. The inorganic hydrated salt was adsorbed onto the surface and pores of colloidal silicon dioxide by physical forces such as surface tension and capillary force, which solved the problem of liquid leakage of inorganic hydrated salts during phase change.

The FT-IR spectra and XRD patterns of colloidal silicon dioxide, $Na_2HPO_4{\cdot}12H_2O$, and composite PCMs are shown in Figure 12. The stretching vibration peaks (1092 cm^{-1}, 865 cm^{-1}, and 529 cm^{-1}) of HPO_4^{2-} and the antisymmetric stretching vibration peaks (1092 cm^{-1}) and bending vibration peaks (468 cm^{-1}) of Si-O-Si could be found in the composite PCMs. According to the characteristic absorption peaks of colloidal silicon dioxide and $Na_2HPO_4{\cdot}12H_2O$, it was found that no new characteristic absorption peak was generated for the composite PCM. Similarly, all the XRD diffraction peaks of composite PCMs could be found in the diffraction peaks of $Na_2HPO_4{\cdot}12H_2O$, although the peak intensity became weak or the peak position moved slightly. This was mainly because the pore structure of colloidal silicon dioxide had a confinement effect on $Na_2HPO_4{\cdot}12H_2O$. Therefore, according to the results of FT-IR and XRD, it could be inferred that there was only physical interaction between the colloidal silicon dioxide and $Na_2HPO_4{\cdot}12H_2O$.

3.5. Thermal Stability. Figure 13 shows the TGA curves of colloidal silicon dioxide, $Na_2HPO_4{\cdot}12H_2O$, and composite PCMs. As colloidal silicon dioxide has strong moisture absorption, its weight loss content corresponded to the moisture content it absorbed, which was 6.04%. For $Na_2HPO_4{\cdot}12H_2O$, its weight loss process corresponded to the loss of crystal water. When the temperature exceeded 340°C, the change of sample mass could be ignored, and the corresponding weight loss was 62.19%. The weight loss process of composite PCMs was similar to that of $Na_2HPO_4{\cdot}12H_2O$. Because the composite PCM contained colloidal silicon dioxide, its total weight loss was less than that of $Na_2HPO_4{\cdot}12H_2O$, which was 45.39%. Based on the weight loss of the three samples, it was clear that the actual content of $Na_2HPO_4{\cdot}12H_2O$ in the composite PCM was 69.6%, which was close to the theoretical value of 70%.

3.6. Thermal Properties. Figure 14 shows the DSC curves of composite PCMs. It can be seen that when no additional

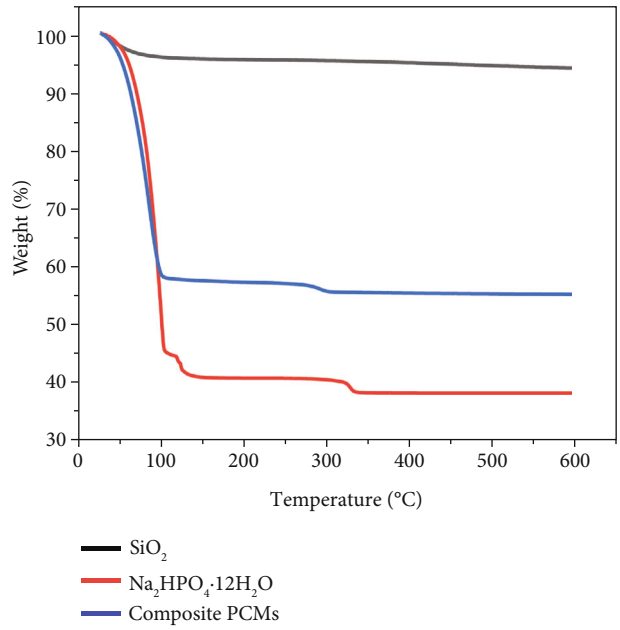

Figure 13: TGA curves of colloidal silicon dioxide, $Na_2HPO_4{\cdot}12H_2O$, and composite PCMs.

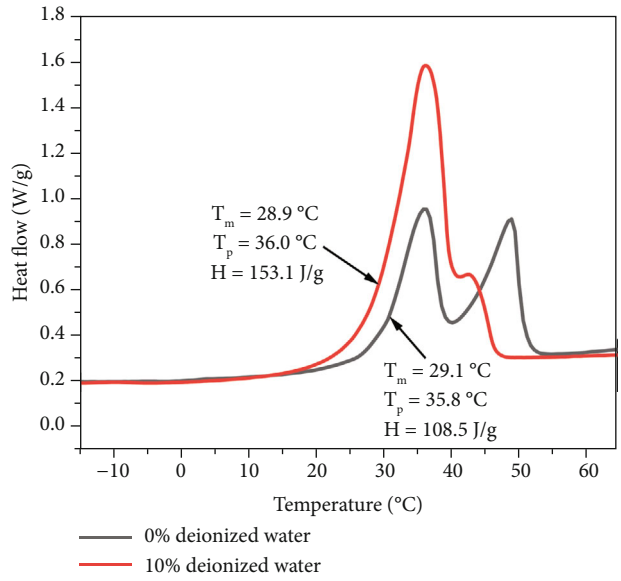

Figure 14: DSC curves of composite PCMs with and without deionized water.

deionized water was added, the enthalpy and phase change temperature of the composite PCMs were 108.5 J/g and 29.1°C, respectively. It was worth mentioning that its DSC curve had two consecutive endothermic peaks, which corresponded to the situation of the cooling curve. That was to say, the thermal properties of composite PCMs were affected by the water loss of hydrated salts. During the preparation of composite PCMs, when 10% deionized water was added, the enthalpy and phase change temperature of composite PCMs were 153.1 J/g and 28.9°C, respectively. The dehydration

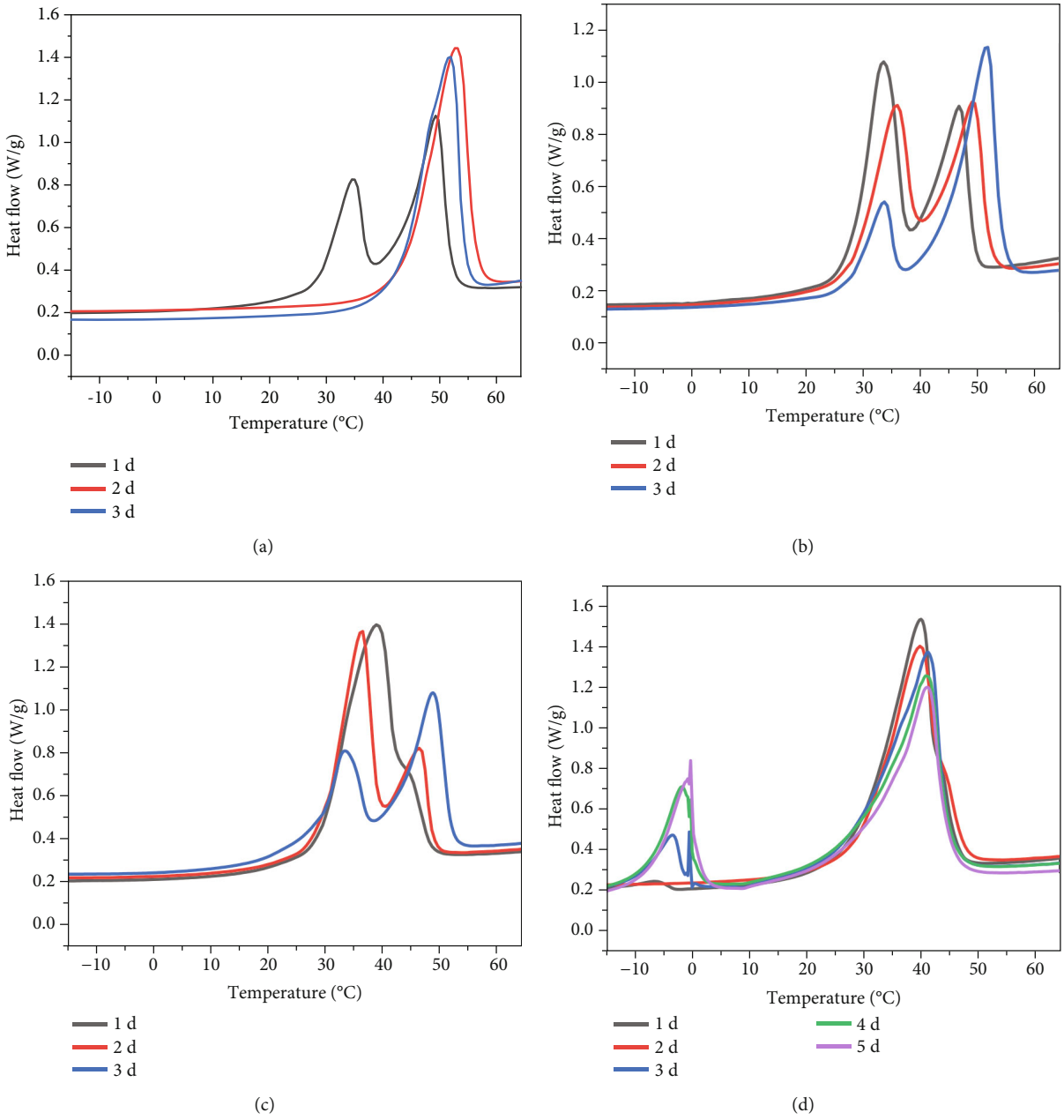

Figure 15: DSC curves of composite PCMs after being placed in different RH for different days: (a) 33%RH; (b) 52%RH; (c) 75%RH; (d) 97%RH.

process is the main source of phase change enthalpy for hydrated salts, and the phase change enthalpy is closely related to the content of crystalline water. The content of crystalline water in hydrated salts should be guaranteed to ensure that it has a high latent heat [36]. $Na_2HPO_4{\cdot}12H_2O$ is prone to weathering under natural conditions, resulting in a decrease in its crystalline water content. The addition of an appropriate amount of deionized water could compensate for the loss of crystalline water and prevent a decrease in enthalpy. It can be seen that adding additional deionized water had little effect on the phase change temperature but greatly improved the heat storage capacity of the composite PCM.

3.6.1. Single Composite PCM Block. The DSC curve of a single composite PCM placed in different RH for different days is shown in Figure 15, and the corresponding thermal characteristics are listed in Table 4. It can be observed that the thermal characteristics of composite PCMs were affected by the RH and the number of days. With the decrease in RH and the increase in days, the water loss of composite PCMs became worse. At 33%RH and 52%RH, two endothermic peaks appeared in the DSC curve of composite PCMs after being placed in the desiccator for one day. And as the number of days increased, the first endothermic peak became smaller and smaller, or even disappeared, while the second endothermic peak became larger and larger. Under

Table 4: Thermal characteristics of composite PCMs after being placed in different RH environments for different days.

RH (%)	Time (d)	T_m (°C)	T_p (°C)	Enthalpy (J/g)
33	1	28.0	49.4	112.0
	2	43.7	52.9	109.2
	3	43.2	51.8	101.1
52	1	28.1	33.6	119.3
	2	28.5	35.9	119.0
	3	27.6	51.6	100.9
75	1	29.0	38.7	143.1
	2	28.9	36.2	125.6
	3	28.6	48.5	111.7
97	1	29.3	40.0	152.0
	2	29.8	39.9	142.3
	3	30.0	41.3	142.1
	4	32.3	40.9	131.4
	5	32.5	41.2	124.7

low RH, the phase change temperature (T_m) and peak temperature (T_p) have changed. Moreover, the enthalpy of composite PCMs was 100~120 J/g, which meant that their thermal storage performance was seriously damaged. At 75%RH, the DSC curve of composite PCMs had only one endothermic peak on the first day. However, with the increase of days, its DSC curve also showed two endothermic peaks, and the enthalpy decreased from 143.1 J/g to 111.7 J/g. At 97%RH, even if the composite PCM was placed in the desiccator for 5 days, its DSC curve did not show two endothermic peaks. As the number of days increased, the phase change temperature increased from 29.3°C to 32.5°C, while the enthalpy decreased from 152.0 J/g to 124.7 J/g. At 97%RH, the process of water absorption instead of water loss took place in the composite PCMs. It can be observed from the DSC curve that the endothermic peak of water became larger and larger with the increase of days. The change of enthalpy and phase change temperature of the composite PCM was small from the first day to the third day. However, when the amount of water absorbed by the composite PCM continues to increase, it would lead to a greater decline in its thermal performance. In general, composite PCMs cannot be exposed to the air environment for a long time.

3.6.2. Sandwich Structure Formed by Composite PCMs and Dried Diatomite. In this part, to investigate the interaction effect between diatomite as a humidity control material and composite PCMs, they were prepared into sandwich structures. It was worth mentioning that diatomite was dried to remove water molecules before preparation, and this structure was recorded as case 1. The thermal characteristics of composite PCMs were tested after the sandwich structure was placed in different humidity for different days. The results are shown in Figure 16 and Table 5. It can be seen that the results obtained were completely different from those above situations, which showed that the presence of diatomite affected the thermal characteristics of composite PCMs. At 33%RH, 52%RH, and 75%RH, the DSC curves of composite PCMs in the sandwich structure had only one endothermic peak. At this time, the phase change temperature was about 44°C, the peak temperature was about 52°C, and the enthalpy was about 100~110 J/g. Similarly, the increase of the phase change temperature and the decrease of the enthalpy indicated that the water loss problem had occurred in composite PCMs. The DSC curves of composite PCMs in the sandwich structure did not show two endothermic peaks, which meant that the dried diatomite accelerated the water loss process of the composite PCM. Because the dried diatomite has moisture absorption capacity, it would absorb water molecules lost by composite PCMs. At 97%RH, after the sandwich structure was placed in the desiccator for one day, the DSC curve of the composite PCM also had only one endothermic peak, and its enthalpy and phase change temperature were 100.6 J/g and 43.8°C, respectively. At this time, the composite PCM was also in a state of water loss. With the increase in the number of days, two endothermic peaks appeared in the DSC curves of composite PCMs, and the first endothermic peak and enthalpy increased gradually. When the number of days reached the fifth day, the DSC curve of the composite PCM now had only one endothermic peak. At this time, the thermal characteristics of composite PCMs were good, and the corresponding enthalpy and phase change temperature were 139.4 J/g and 27.8°C, respectively. The above phenomenon was mainly due to the existence of diatomite in the sandwich structure, which prevented the moisture exchange between the composite PCMs and the humidity environment. In addition, diatomite was dry and would absorb moisture around it. As a result, the composite PCMs in the sandwich structure lost water even at 97%RH at the beginning. However, with the increase of days, diatomite could transfer moisture to composite PCMs after absorbing enough moisture, thus gradually improving the thermal characteristics of composite PCMs.

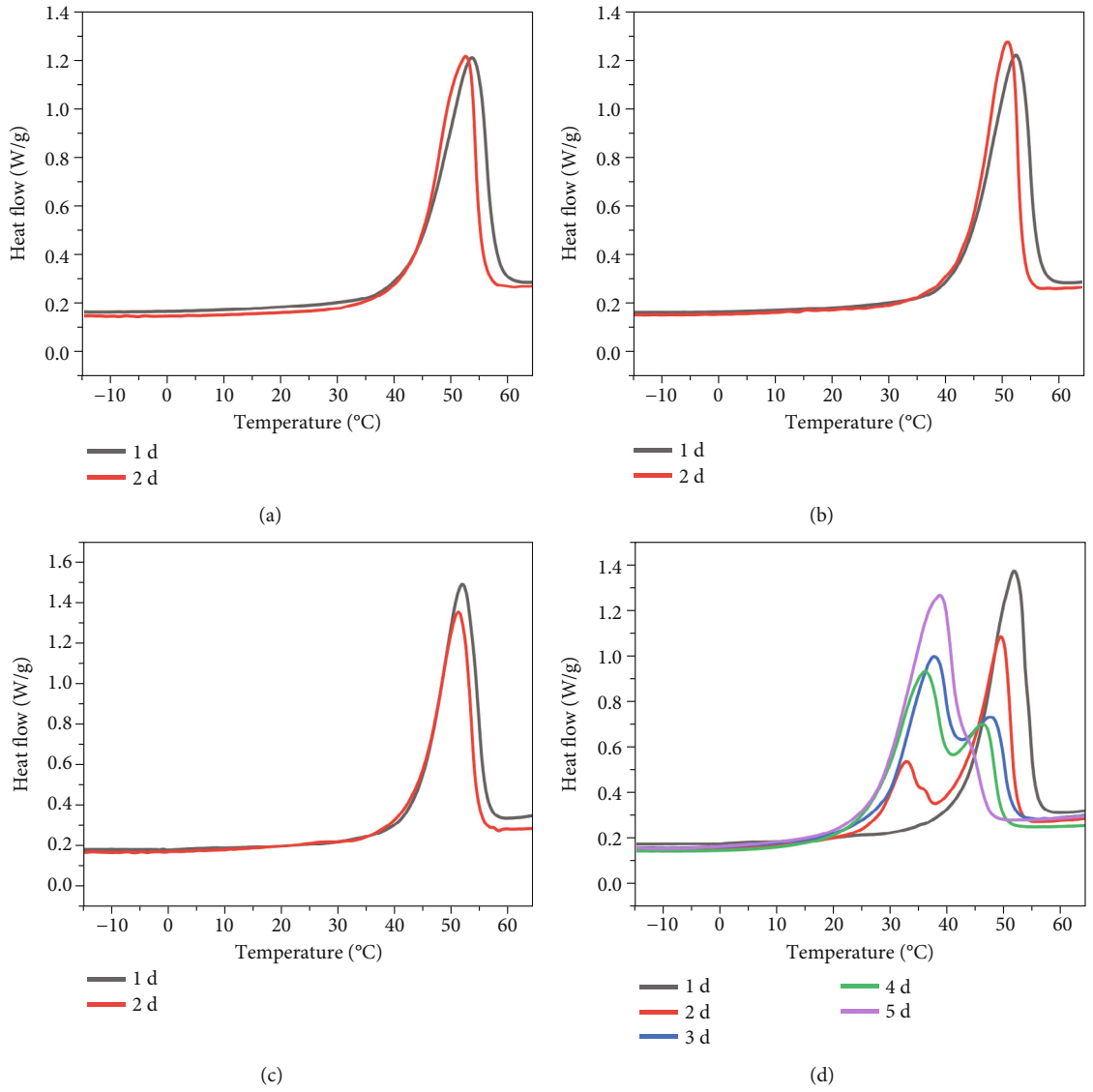

Figure 16: DSC curves of composite PCMs in case 1 after being placed in different RH for different days: (a) 33%RH; (b) 52%RH; (c) 75%RH; (d) 97%RH.

Table 5: Thermal characteristics of composite PCMs in case 1 after being placed in different RH environments for different days.

RH (%)	Time (d)	T_m (°C)	T_p (°C)	Enthalpy (J/g)
33	1	44.0	53.2	103.7
	2	43.8	52.1	95.1
52	1	43.6	52.5	97.6
	2	43.9	51.0	90.1
75	1	44.2	51.7	109.7
	2	44.1	51.1	99.4
97	1	43.8	51.7	100.6
	2	27.3	49.4	96.4
	3	29.4	37.6	124.5
	4	26.9	36.1	126.0
	5	27.8	38.7	139.4

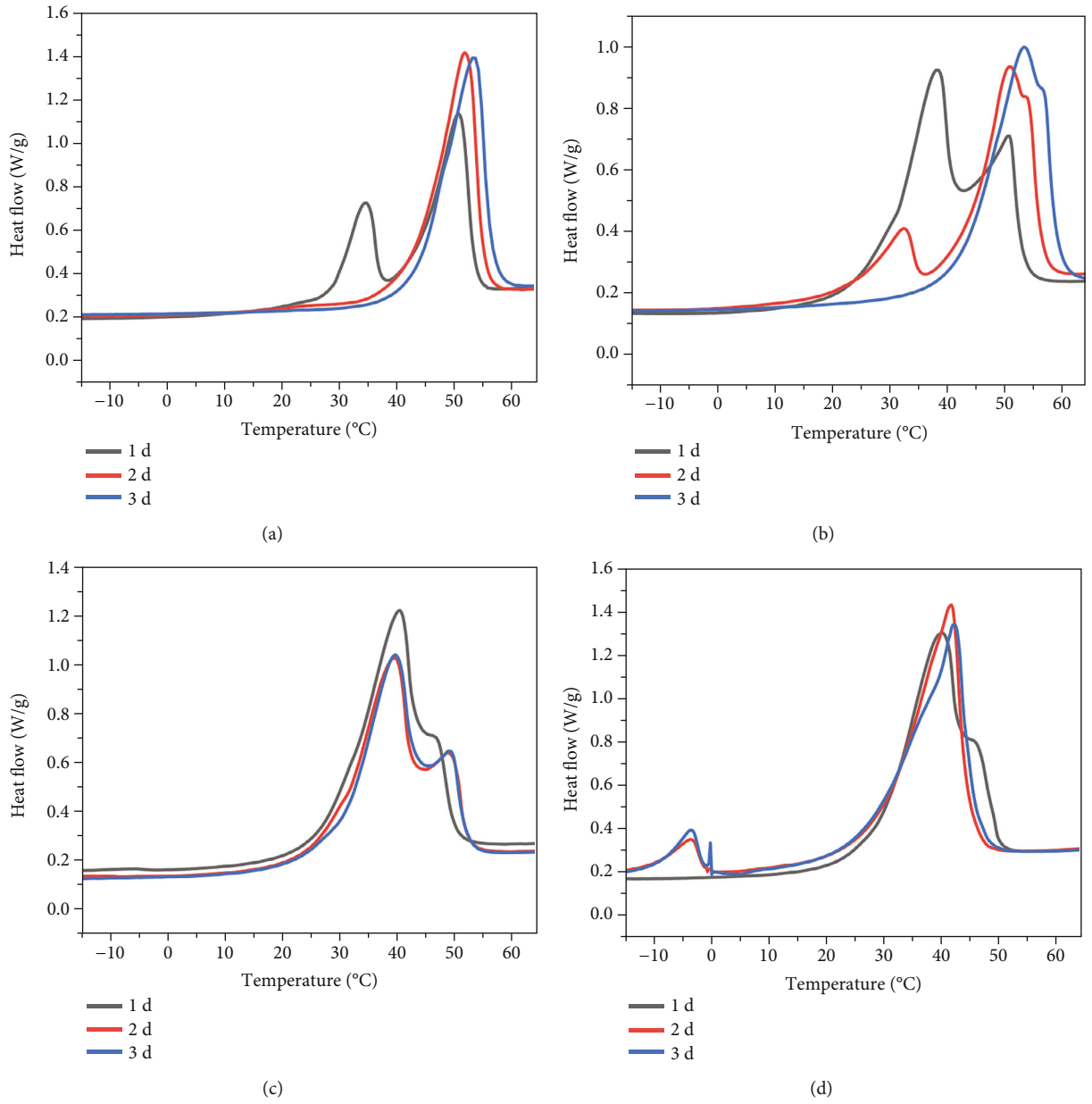

Figure 17: DSC curves of composite PCMs in case 2 after being placed in different RH for different days: (a) 33%RH; (b) 52%RH; (c) 75%RH; (d) 97%RH.

3.6.3. Sandwich Structure Formed by Composite PCMs and Saturated Diatomite. In this part, the diatomite used to prepare the sandwich structure had reached equilibrium moisture content at 97%RH, and the obtained structure was recorded as case 2. The thermal characteristics of composite PCMs were tested after the sandwich structure was placed in different humidity for different days. The results are shown in Figure 17 and Table 6. It can be observed that the DSC curve of composite PCMs was somewhat similar to that in Section 3.6.1. At 33%RH and 52%RH, diatomite would release moisture in the early stage because it had reached the equilibrium moisture content at 97%RH. However, it can be seen from the DSC curve that the release of moisture from diatomite could not improve the water loss process of composite PCMs, and the thermal storage performance of composite PCMs was still poor. At 75%RH, the enthalpy of composite PCMs was larger than that in Section 3.6.1, indicating that the moisture release process of diatomite was conducive to improving the thermal characteristics of composite PCMs. At 97%RH, the moisture saturated diatomite had no obvious influence on the thermal properties of composite PCMs. At this time, the phase change temperature and enthalpy of the composite PCMs on different days were almost the same as those in Section 3.6.1.

In conclusion, humidity control materials would affect the thermal storage performance of composite PCMs. As shown in Figure 18, when the moisture content of diatomite was low, it would absorb the moisture of inorganic hydrated salts, which might have a negative impact on the thermal storage capacity of composite PCMs. However, when the

Table 6: Thermal characteristics of composite PCMs in case 2 after being placed in different RH environments for different days.

RH (%)	Time (d)	T_m (°C)	T_p (°C)	Enthalpy (J/g)
33	1	28.7	50.8	104.5
	2	43.7	51.9	108.6
	3	43.2	53.4	108.6
52	1	29.6	38.2	131.6
	2	24.8	51.0	100.2
	3	42.5	53.4	104.8
75	1	28.8	40.2	148.9
	2	29.8	39.3	134.3
	3	30.7	39.6	130.2
97	1	29.3	40.3	155.9
	2	29.6	41.8	141.9
	3	32.8	42.3	137.5

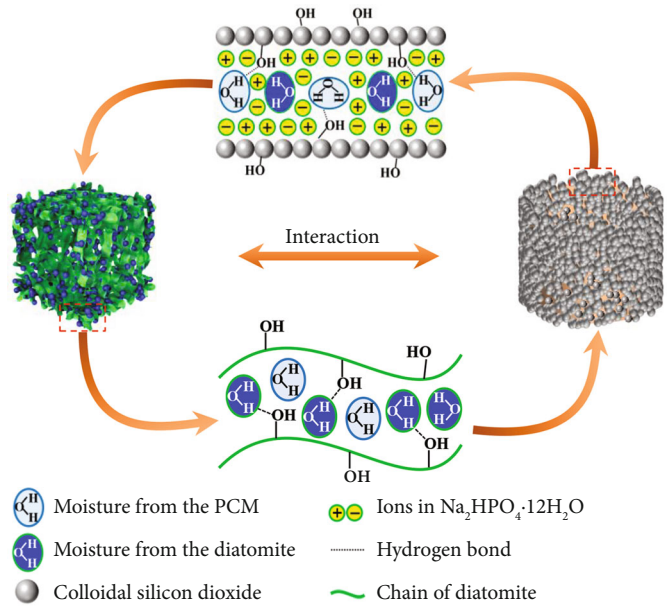

Figure 18: Schematic diagram of the interaction between diatomite and composite PCMs.

moisture content of diatomite was high, the moisture in its pore structure could be transferred to the inorganic hydrated salt during the moisture release process, which slowed down the water loss process of the inorganic hydrated salt. Moreover, from the above results, it can be found that the thermal characteristics of composite PCMs that had lost water were expected to be restored under high RH conditions (Figure 16(d)). It can be speculated that in the environment of alternating high and low RH, the heat storage performance of composite PCMs may not be greatly affected.

3.7. Hygrothermal Performance of the Room Model. The temperature and humidity curves of the reference room and functional room over time are shown in Figure 19. For the reference room, the maximum and minimum temperatures were approximately 40.0°C and 24.3°C, respectively. For the functional room, the highest and lowest temperatures were 39.1°C and 24.8°C, respectively. Although the insulation ability of the temperature and humidity control material was weaker than that of EPS boards, it could still slow down the temperature fluctuations in the room. This was mainly due to the large thermal storage capacity of composite PCMs. During the heating process, composite PCMs absorbed and stored heat, which was beneficial for slowing down heat transfer and lowering temperature. During the cooling process, composite PCMs released the stored heat, thereby increasing the temperature of the room. In terms of humidity regulation, it depended on the absorption and release of moisture by diatomite. For the reference room, the humidity fluctuated between 76%RH and 87%RH. For the functional rooms, the humidity fluctuation further decreased, fluctuating between 77%RH and 82%RH. Diatomite had a

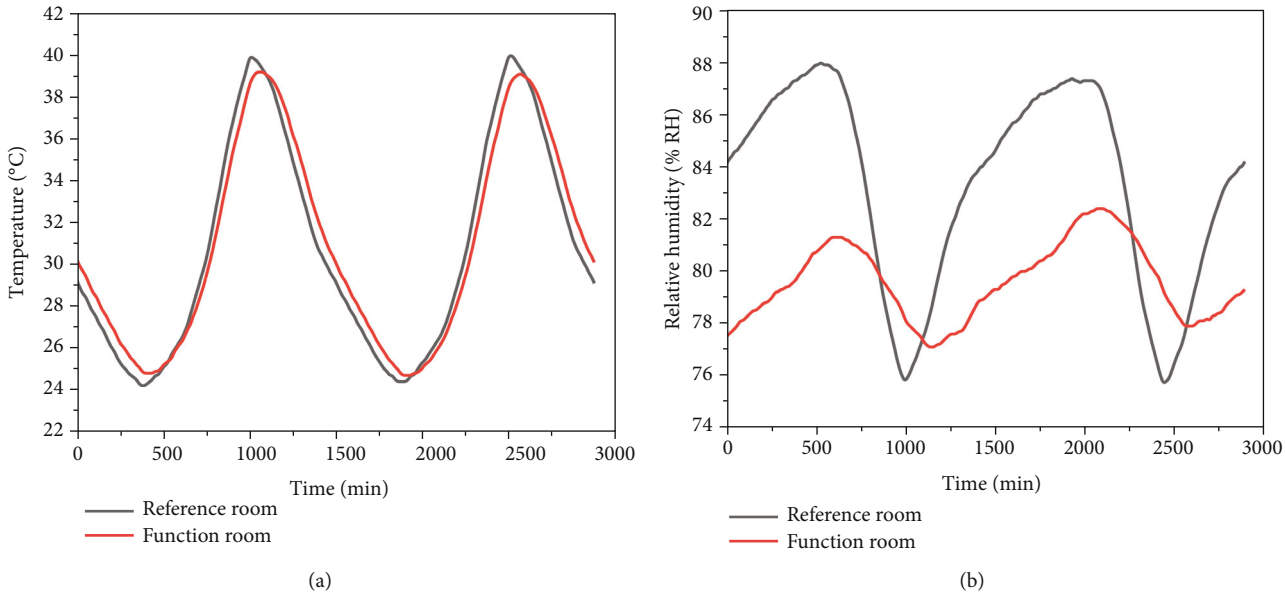

Figure 19: (a) Temperature and (b) humidity curves over time for reference room and functional room.

large specific surface area and rich mesoporous structure. When the RH of the environment was high, diatomite absorbed moisture through surface adsorption and capillary condensation to reduce humidity. When the RH of the environment decreased, diatomite slowed down humidity fluctuations by releasing the absorbed moisture. Therefore, when a portion of the thickness of EPS board was replaced with temperature and humidity control materials, the hygrothermal performance of the room was improved.

4. Conclusions

In this paper, temperature and humidity control materials with the sandwich structure were obtained by combining diatomite and inorganic hydrated salt composite PCMs. As a humidity control material, diatomite had the characteristics of a large specific surface area, rich mesoporous structure, and fast moisture absorption/desorption rate. Its equilibrium moisture content was 0.2173 g/g at 97%RH. In addition, its moisture buffer value was 3.81 g/(m^2·%RH), which had excellent humidity regulation capability. The supercooling of the composite PCM was reduced to 0.8°C by adding 5% $Na_2SiO_3{\cdot}9H_2O$. Through SEM, FT-IR, and XRD tests, it is known that the combination between colloidal silicon dioxide and inorganic hydrated salts was physical adsorption. The TG results showed that the inorganic hydrated salt was easy to loss crystal water. The addition of 10% deionized water enhanced the thermal storage performance of composite PCMs, and the enthalpy increased from 108.5 J/g to 153.1 J/g. The thermal storage performance of single sheet inorganic hydrated salt composite PCMs would decline under a low RH environment, while it would be less affected under a high RH environment. In addition, the absorption and release of moisture by diatomite affected the thermal storage performance of composite PCMs. The dried diatomite would absorb the moisture of inorganic hydrated salt, thus accelerating the water loss process of inorganic hydrated salt. The diatomite with high moisture content could transfer the released moisture to inorganic hydrated salt. The inorganic hydrated salt that had lost water was also expected to recover its heat storage performance after absorbing enough moisture. For the hygrothermal performance of the room model, compared to the reference room, the functional room with temperature and humidity control materials had the ability to regulate the internal temperature and humidity inside the room, which was beneficial for mitigating temperature and humidity fluctuations. Generally, the temperature and humidity control materials obtained in this work can play an important role in environments with high RH.

Data Availability

Data is available on request from the authors.

Conflicts of Interest

The authors declare that they have no conflicts of interest.

Acknowledgments

This work was supported by the National Natural Science Foundation of China (No. 52006250 and No. 52006037) and the Guangdong Basic and Applied Basic Research Foundation (2023A1515140134).

References

[1] P. Wolkoff, "Indoor air humidity, air quality, and health–an overview," *International Journal of Hygiene and Environmental Health*, vol. 221, no. 3, pp. 376–390, 2018.

[2] E. Cuce, D. Harjunowibowo, and P. M. Cuce, "Renewable and sustainable energy saving strategies for greenhouse systems: a

comprehensive review," *Renewable and Sustainable Energy Reviews*, vol. 64, pp. 34–59, 2016.

[3] K. Giannopoulou, I. Livada, M. Santamouris, M. Saliari, M. Assimakopoulos, and Y. Caouris, "The influence of air temperature and humidity on human thermal comfort over the greater Athens area," *Sustainable Cities and Society*, vol. 10, pp. 184–194, 2014.

[4] L. Chun, G. Gong, P. Peng et al., "Research on thermodynamic performance of a novel building cooling system integrating dew point evaporative cooling, air-carrying energy radiant air conditioning and vacuum membrane-based dehumidification (DAV-cooling system)," *Energy Conversion and Management*, vol. 245, article 114551, 2021.

[5] W. W. Che, C. Y. Tso, L. Sun et al., "Energy consumption, indoor thermal comfort and air quality in a commercial office with retrofitted heat, ventilation and air conditioning (HVAC) system," *Energy and Buildings*, vol. 201, pp. 202–215, 2019.

[6] P. K. S. Rathore and S. K. Shukla, "Potential of macroencapsulated PCM for thermal energy storage in buildings: a comprehensive review," *Construction and Building Materials.*, vol. 225, pp. 723–744, 2019.

[7] Y. Zhang, J. Huang, X. Fang, Z. Y. Ling, and Z. G. Zhang, "Optimal roof structure with multilayer cooling function materials for building energy saving," *International Journal of Energy Research*, vol. 44, no. 3, pp. 1594–1606, 2020.

[8] W. Du, H. Fei, Y. Pan, Q. He, J. Zhou, and X. Liang, "Development of capric acid-stearic acid-palmitic acid low-eutectic phase change material with expanded graphite for thermal energy storage," *Construction and Building Materials*, vol. 320, article 126309, 2022.

[9] G. Hekimoğlu, A. Sarı, T. Kar et al., "Carbonized waste hazelnut wood-based shape-stable composite phase change materials for thermal management implementations," *International Journal of Energy Research*, vol. 45, no. 7, pp. 10271–10284, 2021.

[10] E. Tunçbilek, M. Arıcı, M. Krajčík, Y. Li, M. Jurčević, and S. Nižetić, "Impact of nano-enhanced phase change material on thermal performance of building envelope and energy consumption," *International Journal of Energy Research*, vol. 46, no. 14, pp. 20249–20264, 2022.

[11] X. Liu, Z. Huang, Y. Wang et al., "Thermal energy storage and solar energy utilization enabled by novel composite sodium acetate trihydrate/sodium dihydrogen phosphate dihydrate phase change materials," *Solar Energy Materials and Solar Cells*, vol. 247, article 111938, 2022.

[12] T. Guo, G. Sang, Y. Zhang, and X. Cui, "Thermal performance and energy analysis of phase change material-integrated building with the auxiliary heating system in different climate regions," *International Journal of Energy Research*, vol. 2023, Article ID 2518180, 36 pages, 2023.

[13] Y. U. Kim, S. Yang, B. Y. Yun, and S. Kim, "Evaluation of energy consumption in apartment buildings with biochar and phase-change material aggregate-applied artificial stone finishing materials," *International Journal of Energy Research*, vol. 46, no. 9, pp. 12772–12786, 2022.

[14] X. Zhou, H. Jin, A. Gu et al., "Eco-friendly hierarchical porous palygorskite/wood fiber aerogels with smart indoor humidity control," *Journal of Cleaner Production*, vol. 335, article 130367, 2022.

[15] Y. Kang, S. J. Chang, and S. Kim, "Hygrothermal behavior evaluation of walls improving heat and moisture performance on gypsum boards by adding porous materials," *Energy and Buildings*, vol. 165, pp. 431–439, 2018.

[16] Z. Hu, S. Zheng, Y. Tan, and M. Jia, "Preparation and characterization of diatomite/silica composite humidity control material by partial alkali dissolution," *Materials Letters*, vol. 196, pp. 234–237, 2017.

[17] J. H. Park, Y. U. Kim, J. Jeon, B. Y. Yun, Y. Kang, and S. Kim, "Analysis of biochar-mortar composite as a humidity control material to improve the building energy and hygrothermal performance," *Science of the Total Environment*, vol. 775, article 145552, 2021.

[18] B. Zhou, J. Shi, and Z. Chen, "Experimental study on moisture migration process of zeolite-based composite humidity control material," *Applied Thermal Engineering*, vol. 128, pp. 604–613, 2018.

[19] Z. Chen and M. Qin, "Preparation and hygrothermal properties of composite phase change humidity control materials," *Applied Thermal Engineering*, vol. 98, pp. 1150–1157, 2016.

[20] F. Alassaad, K. Touati, D. Levacher, and N. Sebaibi, "Impact of phase change materials on lightened earth hygroscopic, thermal and mechanical properties," *Journal of Building Engineering*, vol. 41, article 102417, 2021.

[21] N. Zhu, X. Li, P. Hu, F. Lei, S. Wei, and W. Wang, "An exploration on the performance of using phase change humidity control material wallboards in office buildings," *Energy*, vol. 239, article 122433, 2022.

[22] X. Wang, Y. Lei, Z. Chen, and W. Lei, "Sepiolite-zeolite powder doped with capric acid phase change microcapsules for temperature-humidity control," *Journal of Colloid and Interface Science*, vol. 595, pp. 25–34, 2021.

[23] Z. Chen, M. Qin, and J. Yang, "Synthesis and characteristics of hygroscopic phase change material: composite microencapsulated phase change material (MPCM) and diatomite," *Energy and Buildings*, vol. 106, pp. 175–182, 2015.

[24] J. H. Park, Y. Kang, J. Lee, S. Wi, J. D. Chang, and S. Kim, "Analysis of walls of functional gypsum board added with porous material and phase change material to improve hygrothermal performance," *Energy and Buildings*, vol. 183, pp. 803–816, 2019.

[25] Z. Zong, D. Chen, C. Zhao et al., "Fabrication and analysis of palmitic acid–decanoic acid@ Ce–Eu/TiO_2 composite as a building material for regulating indoor environment," *Asia-Pacific Journal of Chemical Engineering*, vol. 16, no. 1, article e2575, 2021.

[26] P. Hou, M. Qin, S. Cui, and K. Zu, "Preparation and characterization of metal-organic framework/microencapsulated phase change material composites for indoor hygrothermal control," *Journal of Building Engineering*, vol. 31, article 101345, 2020.

[27] M. Gonçalves, R. M. Novais, L. Senff, J. Carvalheiras, and J. A. Labrincha, "PCM-containing bi-layered alkali-activated materials: a novel and sustainable route to regulate the temperature and humidity fluctuations inside buildings," *Building and Environment*, vol. 205, article 108281, 2021.

[28] A. A. A. Abuelnuor, A. A. M. Omara, K. M. Saqr, and I. H. I. Elhag, "Improving indoor thermal comfort by using phase change materials: a review," *International Journal of Energy Research*, vol. 42, no. 6, pp. 2084–2103, 2018.

[29] B. Kalidasan, A. K. Pandey, R. Saidur, S. K. Tyagi, and Y. K. Mishra, "Experimental evaluation of binary and ternary eutectic phase change material for sustainable thermal energy storage," *Journal of Energy Storage*, vol. 68, article 107707, 2023.

[30] B. Kalidasan, A. K. Pandey, R. Saidur, R. Kothari, K. Sharma, and V. V. Tyagi, "Eco-friendly coconut shell biochar based

nano-inclusion for sustainable energy storage of binary eutectic salt hydrate phase change materials," *Solar Energy Materials and Solar Cells*, vol. 262, article 112534, 2023.

[31] B. Kalidasan, A. K. Pandey, R. Saidur, M. Samykano, and V. V. Tyagi, "Nano additive enhanced salt hydrate phase change materials for thermal energy storage," *International Materials Reviews*, vol. 68, no. 2, pp. 140–183, 2023.

[32] W. Sun, G. Liang, F. Feng, H. He, and Z. Gao, "Study on sodium acetate trihydrate-expand graphite-carbon nanotubes composite phase change materials with enhanced thermal conductivity for waste heat recovery," *Journal of Energy Storage*, vol. 55, article 105857, 2022.

[33] Y. Wang, J. Sui, and Z. Xu, "Preparation and characterization of $CaCl_2{\cdot}6H_2O$ based binary inorganic eutectic system for low temperature thermal energy storage," *Energy*, vol. 259, article 125036, 2022.

[34] R. Ye, H. Jiang, J. Wang, X. Yang, and X. Shu, "Fabrication and characteristics of eutectic hydrated salts/fumed silica composite as form-stable phase change materials for thermal energy storage," *Solar Energy Materials and Solar Cells*, vol. 238, article 111584, 2022.

[35] D. Xing, C. Dong, Z. Li et al., "Preparation and characterization of sodium sulfate decahydrate–sodium acetate trihydrate shape-stabilized phase change materials," *Energy & Fuels*, vol. 36, no. 9, pp. 4947–4956, 2022.

[36] Y. Li, C. Li, N. Lin, B. Xie, D. Zhang, and J. Chen, "Review on tailored phase change behavior of hydrated salt as phase change materials for energy storage," *Materials Today Energy*, vol. 22, article 100866, 2021.

[37] Z. Rao, T. Xu, C. Liu, Z. Zheng, L. Liang, and K. Hong, "Experimental study on thermal properties and thermal performance of eutectic hydrated salts/expanded perlite form-stable phase change materials for passive solar energy utilization," *Solar Energy Materials and Solar Cells*, vol. 188, pp. 6–17, 2018.

[38] C. Rode, R. H. Peuhkuri, L. H. Mortensen, and P. Vlček, *Moisture Buffering of Building Materials*, Technical University of Denmark, Department of Civil Engineering, 2005.

[39] C. Rode, R. Peuhkuri, B. Time, K. Svennberg, and T. Ojanen, *Moisture buffer value of building materials*, ASTM International, 2007.

[40] Z. Hu, S. Zheng, M. Jia, X. Dong, and Z. Sun, "Preparation and characterization of novel diatomite/ground calcium carbonate composite humidity control material," *Advanced Powder Technology*, vol. 28, no. 5, pp. 1372–1381, 2017.

[41] Z. Hu, S. Zheng, Z. Sun, Y. Chen, and Y. Yan, "Influence of pore structure on humidity control performance of diatomite," *Science and Technology for the Built Environment*, vol. 23, no. 8, pp. 1305–1313, 2017.

[42] W. Jia, C. Wang, T. Wang, Z. Cai, and K. Chen, "Preparation and performances of palmitic acid/diatomite form-stable composite phase change materials," *International Journal of Energy Research*, vol. 44, no. 6, pp. 4298–4308, 2020.

[43] L. Que and X. Zhang, "Experimental investigations on the thermal performance and phase change hysteresis of composite phase change material $Na_2HPO_4{\cdot}\ 12H_2O/SiO_2$," *Journal of Energy Storage*, vol. 54, article 105360, 2022.

[44] P. Dixit, V. J. Reddy, S. Parvate et al., "Salt hydrate phase change materials: current state of art and the road ahead," *Journal of Energy Storage*, vol. 51, article 104360, 2022.